Supplementary Figures

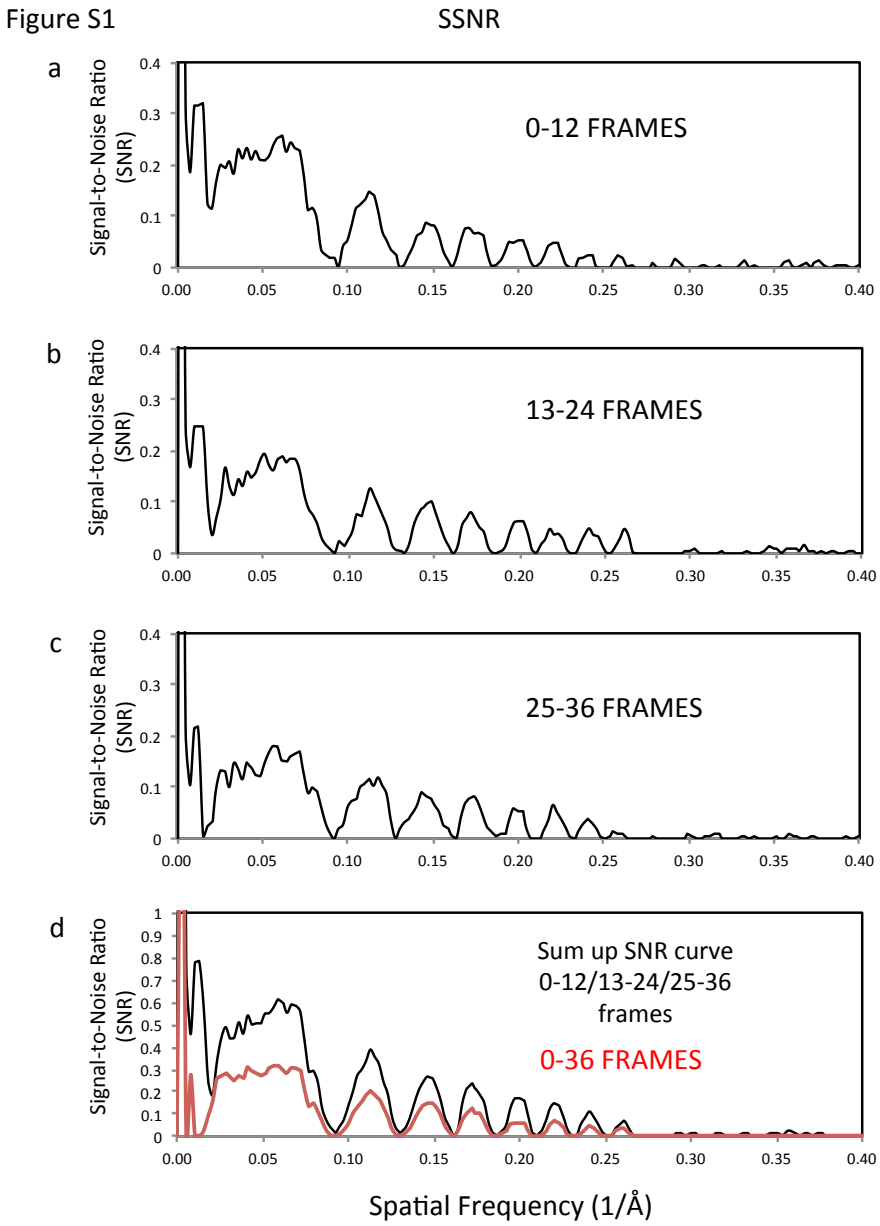

***Supplementary Fig. 1*:** SSNR of individual sub-averages of 12 frames (a-c) throughout a single exposure series. (d) Sum of the three resulting curves of a-c (black) and the SSNR of a straight sum of 0-36 frames (red).

Figure S2

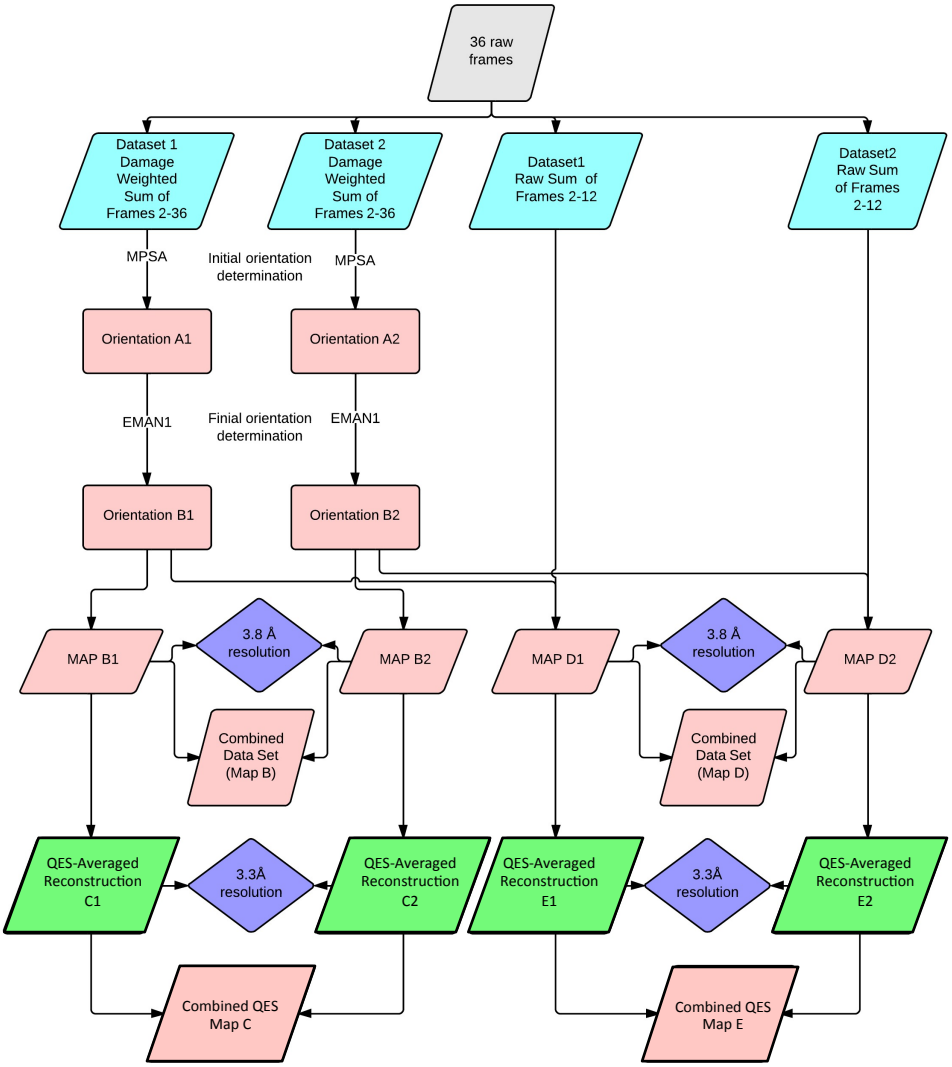

Supplementary Fig. 2: Flowchart of BMV data processing and independent reconstructions of two data sets. After processing raw movie data (grey), particle images were generated based on damage compensated data (frames 2-26) and a sum of frames 2-12 (cyan). Refinement (pink) was done by MPSA and *EMAN1*. Final resolution determination (blue) is determined by 0.143 of gold-standard FSC curve. Quasi-equivalent subunit (QES) averages maps (green) are aligned by *Foldhunter*.

Figure S3

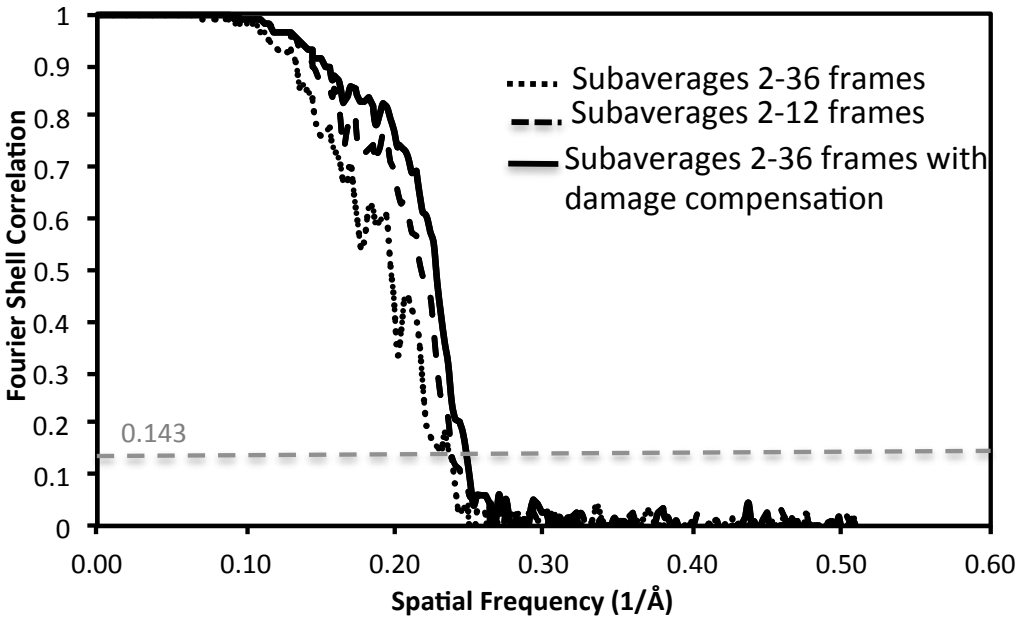

Supplementary Fig. 3: Fourier shell correlation (FSC) curves for reconstructions computed from particle images generated by summing various numbers of frames, with and without damage compensation.

Figure S4

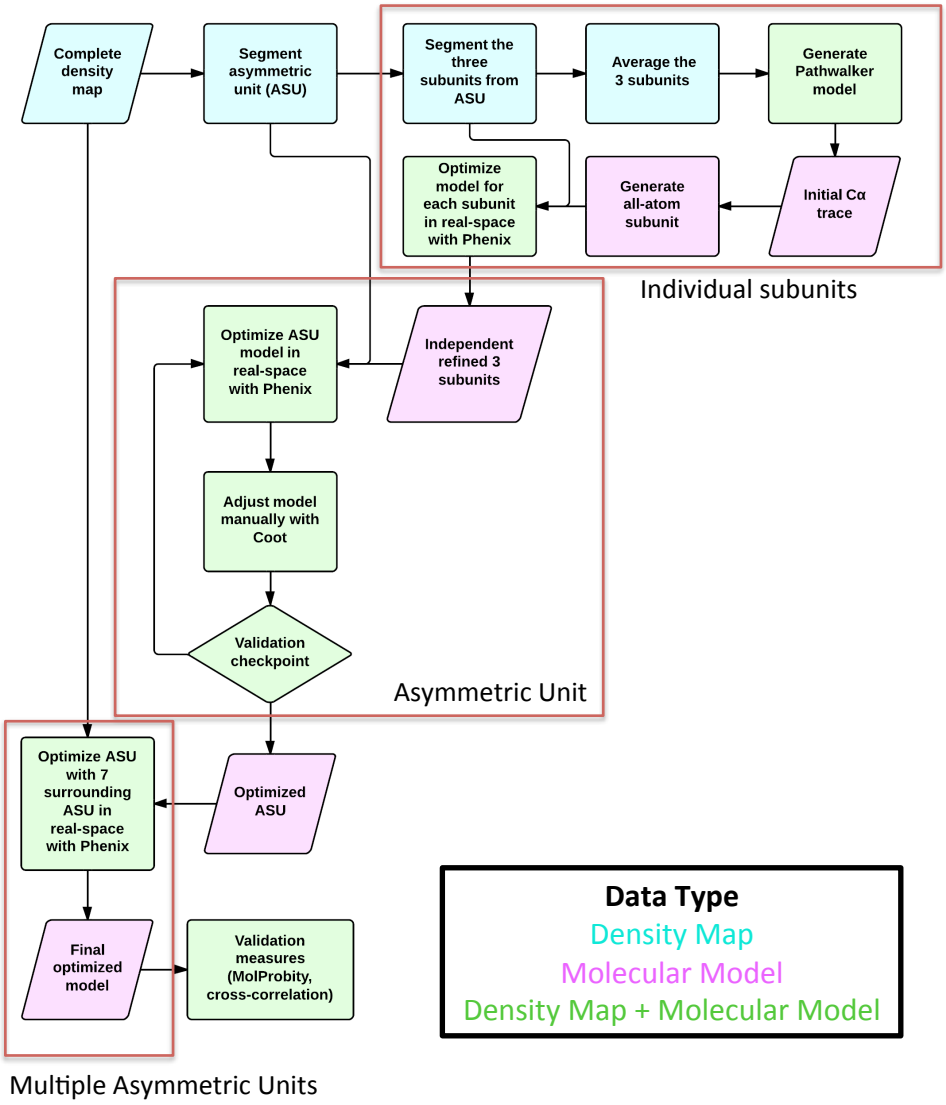

Supplementary Fig. 4: Flowchart for generating optimized molecular models from BMV density map. Following segmentation, quasi-equivalent subunit (QES) averaging was done to begin *de novo* modeling pipeline, which included *Pathwalker* and *Gorgon*. Once a Cα model was generated, it was converted to an all-atom subunit and optimized with the *Phenix* real-space refine routine. The all-atom model was first optimized for individual subunit densities; once complete a large complex (asymmetric unit) was assembled and optimized in a similar fashion. This process used surrounding asymmetric

units to optimize interfaces between the asymmetric unit and its neighbors. The final model was validated by *MolProbity* and cross-correlation.

Figure S5

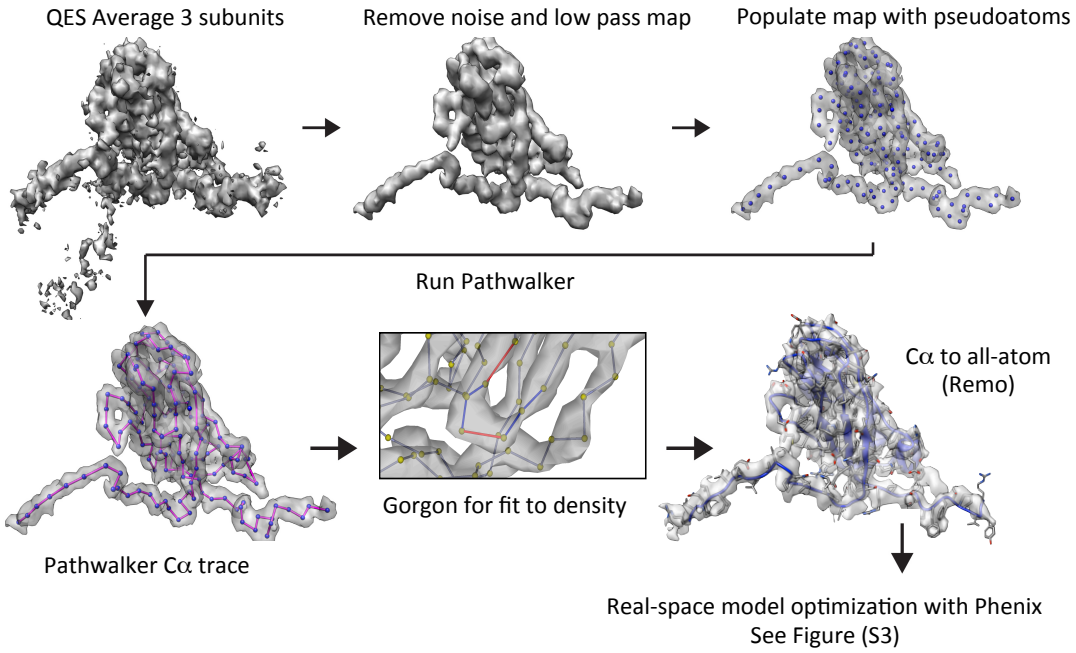

Supplementary Fig. 5: The *de novo* modeling pipeline. QES averaging was used to remove noise and improve connectivity for fold determination. The *Pathwalker* protocol was then used to generate a Cα trace, which was improved with *Gorgon* and subsequently converted to an all-atom model.

Figure S6

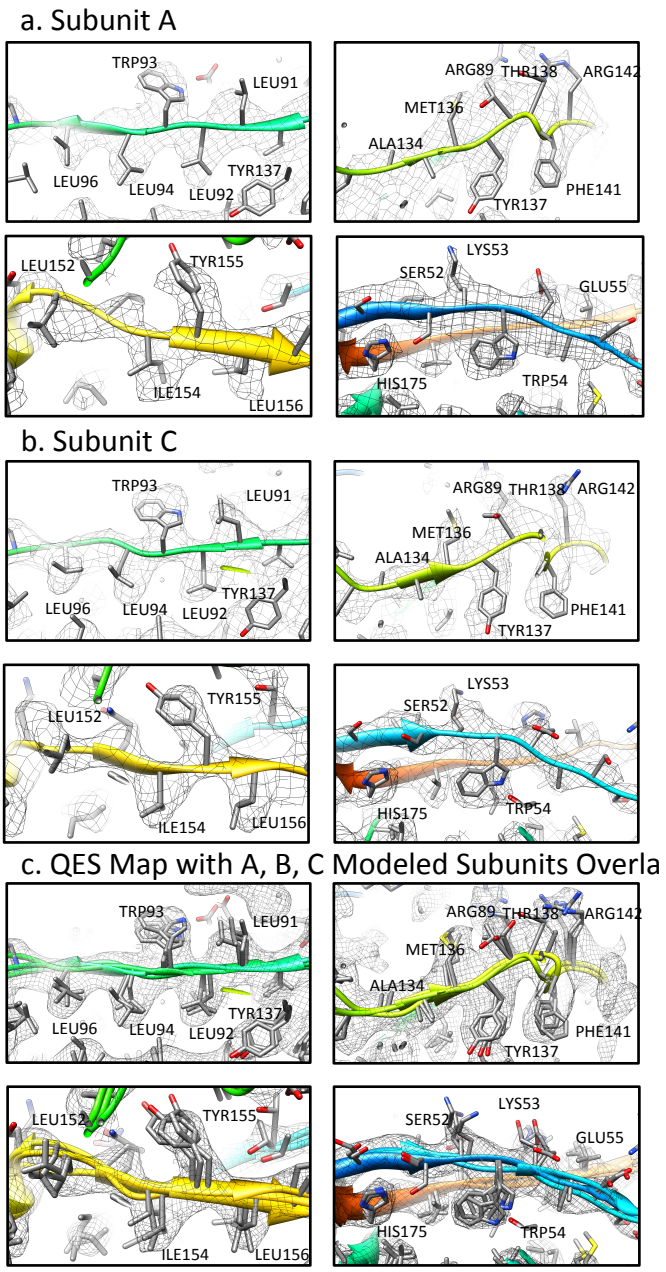

Supplementary Fig. 6: Additional side chain images from subunit A (a) and C (b) (the corresponding regions in subunit B shown in Fig. 5). (c) The QES averaged density map with optimized models derived from the three overlapped capsid subunits

Figure S7

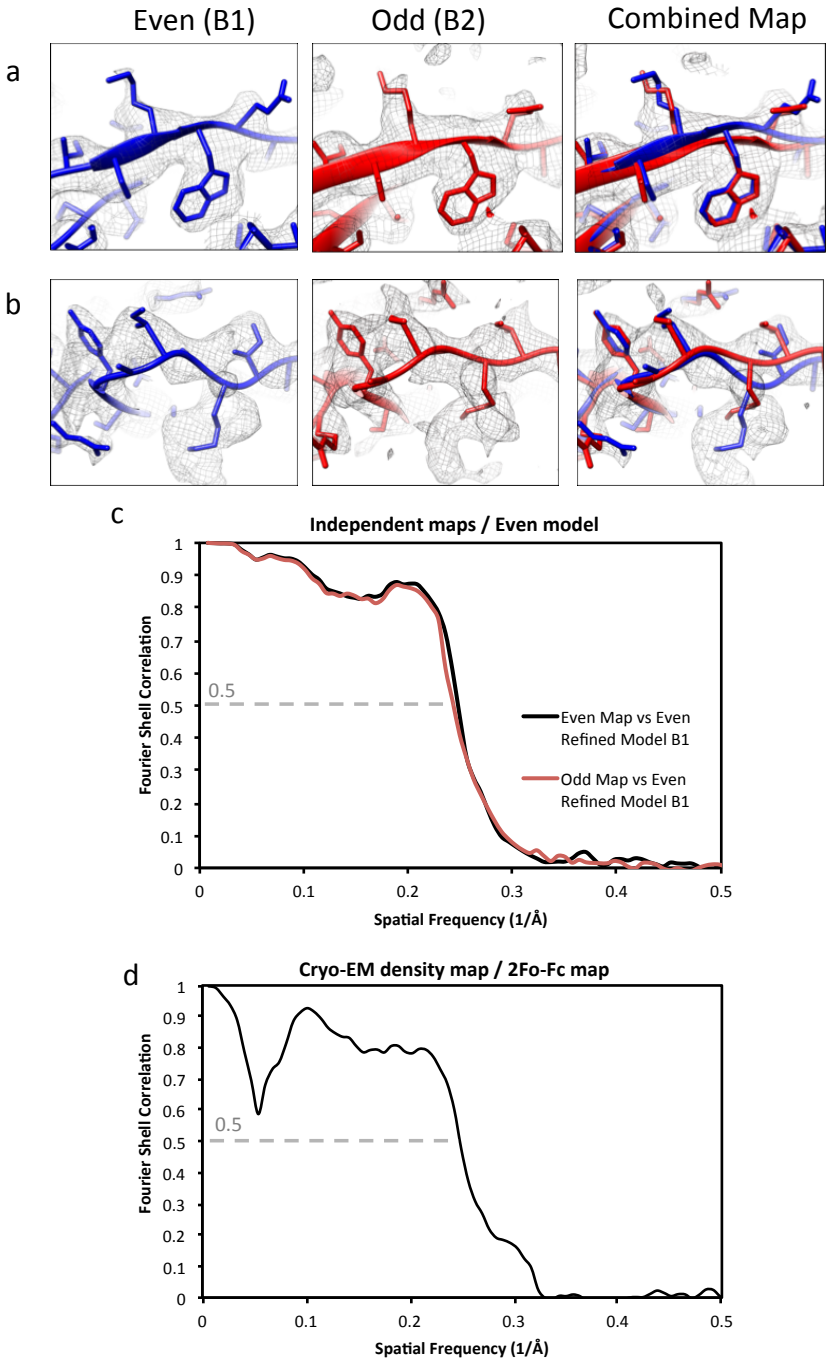

Supplementary Fig. 7: Model variation between two independent models derived from the independent data sets. (a) Side chain view of a region with two similar data derived

data sets from independent maps. The combined map is shown in the right panel with the two models overlapped. (b) Side chain view of a region in the CP with two models derived from independent maps. This region shows variation due to the quality of the density map. The combined map is shown in the right panel with the two overlapping models. (c) Two FSC curves comparing simulated density from one half data set model (model B1) to the two independent split density maps. (d) FSC curve between an asymmetric unit of our derived cryo-EM experimental density map and a map generated from the deposited X-ray structure factors.